Cortical neuronal activity determines the dynamics of local sleep homeostasis

Christopher W. Thomas[1], Mathilde C. C. Guillaumin[2], Laura E. McKillop[1],

Peter Achermann[3], Vladyslav V. Vyazovskiy[1]*

[1] Department of Physiology, Anatomy and Genetics, University of Oxford, Oxford, UK; [2] Nuffield Department of Clinical Neurosciences, University of Oxford, Oxford, UK; [3] The KEY Institute for Brain-Mind Research, Department of Psychiatry, Psychotherapy and Psychosomatics, University Hospital of Psychiatry, Zurich, Switzerland

* Corresponding author. Email: vladyslav.vyazovskiy@dpag.ox.ac.uk

Funding acknowledgements**:** BBSRC (BB/K011847/1, BB/M011224/1), MRC (MR/L003635/1), Wellcome Trust (098461/Z/12/Z), John Fell OUP Research Fund (131/032).

Abstract

The homeostatic regulation of sleep manifests as a relative constancy of its total daily amount, and the compensation of sleep loss by an increase in its subsequent duration and intensity. Theoretical descriptions of this phenomenon define "Process S", a variable with dynamics dependent only on sleep-wake history and whose levels are reflected in EEG slow wave activity. While numerous hypotheses have been advanced regarding the substrate and role of Process S, such as synaptic or energy homeostasis, it remains unclear whether these dynamics are fundamentally driven by a need to homeostatically regulate specific variables, or by an unknown innate process which enforces that a certain daily sleep quota is obtained. Sleep is typically defined based on brain-derived criteria, such as behaviour or EEG power spectra, and variation in brain activity during wakefulness has been linked to variation in Process S accumulation. We therefore hypothesised that Process S dynamics might be related to the quantity and characteristics of spiking activity in cortical neurones. Specifically, we assumed that Process S changes as a function of the deviation of neuronal firing rate from a locally defined set point. To relate these dynamics explicitly to patterns of spiking activity, we incorporated the occurrence of network spiking off periods as both the defining measure of Process S and as the determinant of its rate of decay. This approach was able to describe the time course of Process S, crucially without explicit knowledge of the animal's global sleep-wake state. This work provides a conceptual advance in our understanding of the substrate of sleep homeostasis and provides important links between local and global aspects of sleep regulation.

Introduction

According to traditional theory, the need for sleep accumulates during wakefulness and dissipates during sleep. Despite decades of research, it is still uncertain precisely which biological variables form the substrate of sleep need, what characteristics of wake challenge their stability and how sleep mediates the restoration of homeostasis. More fundamentally, it remains unclear whether homeostatic sleep regulation reflects an active process, dynamically shaping daily sleep architecture in response to a physiological need for the homeostatic regulation of specific variables, or whether it corresponds instead to an unknown innate process which ensures only that a certain daily quota of sleep is obtained.

The earliest theories of sleep homeostasis supposed the existence of a single variable, termed Process S, which describes sleep drive at the global level (Borbély, 1982). This variable is assumed to always increase during wakefulness, independently of its content, and to decline during sleep. It is widely acknowledged that homeostatic sleep pressure is reflected in the levels of slow wave activity (SWA, 0.5-4 Hz spectral power) observable during NREM sleep in neurophysiological field potentials, such as electroencephalogram (EEG) or local field potential (LFP).

Current views on the origin of sleep homeostasis emphasise its local and activity-dependent component (Krueger & Tononi, 2011; Rattenborg et al., 2012; Tononi & Cirelli, 2014). It was shown that SWA is far from uniform across the brain, and that the behavioural and cognitive content of waking, beyond merely its duration, influences subsequent SWA magnitude (Huber et al., 2004; Vyazovskiy & Tobler, 2008; Rector et al., 2009; Murphy et al. 2011; Fisher et al., 2016). Indeed, many candidate mechanisms for the substrate of sleep homeostasis implicate processes occurring at a cellular and network level. These include the maintenance of cellular homeostasis (Reimund 1994; Mackiewicz et al., 2007; Vyazovskiy & Harris, 2013; Bellesi et al., 2016), the replenishment of energy stores (Scharf et al., 2008), the influence of sleep-related signalling molecules such as adenosine or cytokines (Krueger et al., 2008), and the regulation of imbalanced synaptic strength (Tononi & Cirelli 2003; Vyazovskiy et al., 2008; Liu et al., 2010). Although the equivalence of these processes with Process S has not been conclusively demonstrated (Frank & Heller, 2019), the existing evidence supports the relevance of sleep-wake dependent differences in neuronal activity for understanding the regulation of sleep.

Cortical neuronal activity is generally higher during waking compared to sleep (Vyazovskiy et al., 2009; Hengen et al., 2016; McKillop et al., 2018). Lower spike firing typical of sleep is due, at least in part, to regular periods of widespread synchronous network silence, termed off periods, intruding on ongoing activity (Steriade et al., 1993a; Steriade et al., 2001; Sanchez-Vives & Mattia, 2014). Importantly, off periods in neural populations are thought to underpin slow wave dynamics at the level of the field potential (Steriade et al., 1993b; Massimini et al., 2004; Buzsáki et al., 2012) and their properties reflect homeostatic sleep need (Vyazovskiy et al., 2009; McKillop et al., 2018; Saberi-Moghadam et al., 2018).

Neuronal firing rates typically fluctuate around a homeostatic set point, which is characteristic for individual cells and variable across the population (Turrigiano, 2011; Hengen et al., 2013; O'Leary et al., 2014; Styr et al., 2019). The homeostatic regulation of firing rates may depend on processes occurring specifically in sleep and wakefulness (Grosmark et al., 2012; Hengen et al, 2016) and evidence suggests that firing rates change as a function of time spent awake, conditional on wake's behavioural quality (Vyazovskiy et al., 2009; Fisher et al., 2016). Additionally, the magnitude and direction of state-dependent changes in firing rate differs between neurons, depending on brain region and their individual firing rate set point (Miyawaki & Diba 2016; Watson et al., 2016; Miyawaki et al., 2019). Firing rate homeostasis may occur above the individual cell level (Slomowitz et al., 2015), as network level mechanisms dependent on the NREM sleep slow oscillation constrain the distribution of population firing rates within an optimal functional range (Levenstein et al., 2017).

Overall, evidence suggests that the homeostatic regulation of sleep and of neuronal firing rates may be intrinsically related, however, this functional link remains incompletely defined. Mathematical modelling approaches present an opportunity to begin addressing this problem. To this end, we develop quantitative models of Process S, describing its temporal dynamics on a local level in terms of spiking activity and off periods, instead of global sleep-wake history. We find that the magnitude of the deviation of multi-unit firing rate from a locally specified set point carries sufficient information to account for empirically derived patterns of SWA. We then introduce the total time spent in off periods as an alternative measure for Process S with more local origins than SWA, and account for the time course of this variable in terms of two opponent processes dependent on spiking rate and off period occurrence.

Materials & Methods

Animals, surgery & husbandry

Chronic electrophysiological recordings from six male young adult (4.8 – 5.7 months old, mean 5.2 months) C57BL/6J mice were analysed here. This data set is a subset of that used in a previous study (McKillop et al., 2018). The animals were surgically implanted with electrodes for the continuous recording of electroencephalography, electromyography and cortical neuronal activity. EEG screw electrodes (Fine Science Tools) were inserted into the skull unilaterally above the frontal cortex (primary motor area: anteroposterior 2mm, mediolateral 2mm) and bilaterally above the occipital (primary visual area: anteroposterior 3.5mm, mediolateral 2.5mm) cortex. One occipital screw (contralateral to the frontal screw) served as the ground electrode and an additional screw located above the cerebellum served as the reference. A pair of stainless steel wires were inserted into nuchal muscle for the recording of electromyogram (EMG). A polyimide-insulated tungsten microwire array (Tucker-Davis Technologies) was implanted through a craniotomy window into the frontal cortex (primary motor area: anteroposterior 2mm, mediolateral -2mm), contralateral to the EEG screw. The array comprised 16 wire channels of 33μm diameter, arranged in 2 rows of 8, with columnar separation of 250μm, row separation of 375μm and tip angle of 45 degrees. One row of wires was 250μm longer than the other to account for cortical curvature. A silicone gel (KwikSil, World Precision Instruments) was used to seal the craniotomy, and dental acrylic cement used to stabilise all the implanted electrodes. Surgeries were performed under isoflurane anaesthesia (4% induction, 1-2% maintenance). Analgesics were given immediately before surgery (1-2 mg/kg metacam and 0.08 mg/kg vetergesic, subcutaneous injection) and for at least 3 days during recovery following surgery (1-2 mg/kg metacam, oral). In addition, immunosuppressant (0.2 mg/kg dexamethasone) was given the day before surgery (oral), immediately before surgery (subcutaneous injection) and during recovery for at least 2 days (oral). Animal wellbeing was closely monitored during recovery until a stable return to baseline was observed for at least 2 days. All procedures were performed under a UK Home Office Project License and conformed to the Animal (Scientific Procedures) Act 1986.

Mice were housed individually following surgery. Two weeks after surgery, mice were transferred, still individually, to custom made Plexiglas cages (20.3x32x35 cm), containing a running wheel (Campden Instruments), which were placed within ventilated sound-attenuated Faraday chambers (Campden Instruments). The animals were exposed to a standard 12hr-12hr light dark cycle, with food and water available *ad libitum*. Mice were allowed to habituate to the recording chamber and to attachment of the recording cables for a minimum of three days before recordings began.

Experimental design

All the data analysed here were collected over two days of experimental recording. The first day served as a baseline, while the animals were completely undisturbed. A sleep deprivation protocol was enforced at light onset on the second day, immediately after the baseline day, and lasted 6 hours. Sleep deprivation was performed using novel object presentation. During this period, experimenters constantly monitored both the behaviour and ongoing neurophysiological recordings of the mice. As soon as any animal showed signs of sleepiness (such as stillness with eyes closed, or slow waves in the EEG), novel objects were introduced to the cage (such as cardboard, colourful plastic and tissue paper) in order to encourage wakefulness. During the 6-hr sleep deprivation period, these mice slept 6.0 ± 3.1 minutes (mean ± sd) only.

Data collection & pre-processing

Data acquisition was performed using a Multichannel Neurophysiology Recording System (Tucker Davis Technologies). EEG, EMG and microwire array LFP signals were filtered (0.1-100 Hz), amplified (PZ5 NeuroDigitizer preamplifier, TDT) and stored locally (256.9 Hz sampling rate). Custom written Matlab scripts were used for signal conversion and data pre-processing. The LFP, EMG and EEG signals were filtered again offline between 0.5 - 100 Hz (4th order Type II Chebyshev filter) and resampled at 256 Hz.

Extracellular multi-unit spiking was additionally obtained from each microwire array channel, recorded at 25 kHz and filtered 300 Hz – 5 kHz. An amplitude threshold (at least 2 standard deviations, minimum -25μV) was used to identify putative spikes. Individual spikes were saved as a voltage waveform comprising 46 data samples (0.48ms before to 1.36ms after threshold crossing) plus a time stamp of

occurrence. Spiking activity from each channel was cleaned offline for artefacts using the Matlab spike sorting software Wave_clus (Quiroga et al., 2004). All putative single unit clusters identified by the algorithm from the same channel were merged, excluding only noise spikes. MUA firing rate for each channel was calculated in 4-second epochs as the mean number of spikes per second.

Vigilance states were scored manually by visual inspection with a 4-second epoch resolution (using the software SleepSign, Kissei Comtec). Vigilance states were classified as waking (low amplitude but high frequency EEG with high or phasic EMG activity), NREM sleep (presence of EEG slow waves, a signal of a high amplitude and low frequency, and a low level of EMG activity) or REM sleep (low amplitude, high frequency EEG, and low EMG). For this analysis, over the six mice, a total of 78 out of 96 channels could be analysed (minimum of 10 out of 16 from one mouse). The excluded channels were characterised by an unstable MUA firing rate, including a large drift in firing which was persistent and sleep-wake state independent. For the off occupancy models described below, 75 out of 96 channels were used; a further 3 channels had to be excluded because multi-unit firing rates, while stable, were too low to yield a reasonable estimate of the occurrence of off periods.

Slow wave activity

Each EEG and LFP signal was processed to extract a measure of the SWA. Signal segments were extracted within windows of 4-second duration and 1-second spacing (giving 3-second overlap), and Hann tapered. A Fourier Transform was applied to each signal segment and the mean power in the slow wave range (frequencies from 0.5 to 4 Hz) was calculated. This measure was smoothed by finding the median over five temporally adjacent overlapping segments, yielding a SWA measurement for each sequential 4 second epoch. For normalisation within each channel, SWA values were then expressed as a percentage of the mean SWA calculated over all artefact-free epochs scored as NREM sleep in the baseline 24 hours. The median value of the SWA during each continuous NREM sleep episode served as an estimate of Process S. NREM sleep episodes shorter than 1 minute (15 epochs) were excluded, as in a previous study modelling Process S in mice (Guillaumin et al., 2018). Brief awakenings (short arousals accompanied by movement, lasting ≤20 seconds) were excluded from analysis but were not considered to be the ending of a NREM sleep episode.

163 **Off periods detection and definition of "off occupancy"**

164 One aim of this study was to develop measures of Process S independent of the EEG, and so we focused
165 on off periods which are the neuronal counterpart of slow waves. Off periods refer to brief interruptions
166 of spiking activity which occur synchronously across many recording sites, last approximately 70-
167 100ms (Vyazovskiy et al., 2009), and are coincident with the positive deflection of LFP slow waves
168 (McKillop et al., 2018). In these studies, off periods were detected by pooling spikes over all channels
169 and identifying inter-spike intervals (ISIs) that exceed some long duration threshold. However, pooling
170 spikes removes the ability to compare local differences, and if an off period does not involve all channels
171 it will go undetected. To overcome this limitation, off periods were defined separately for each channel
172 by looking at the co-occurrence of local slow waves and spiking silence.

173 There is no universally accepted method for slow wave detection, and a recent comparison suggests that
174 a simple amplitude threshold based approach, while in theory adequate, may underperform due to
175 channel differences in overall LFP amplitude and large amplitude fluctuations of higher frequencies
176 (Bukhtiyarova et al., 2019). For this reason, the LFP was first filtered from 0.5 to 6 Hz (4th order
177 Butterworth filter), and a threshold defined individually for each channel, using the median plus one
178 median absolute deviation of the peak amplitude of all positive half waves (including all vigilances
179 states, but excluding epochs with artefacts). All positive half waves with peak amplitude above threshold
180 were then considered to be slow waves.

181 Next, for each LFP slow wave, the multi-unit spike preceding and following the slow wave peak was
182 identified and the corresponding ISI determined. The distribution of these ISIs which coincide with slow
183 waves was often (in 64 out of 75 channels) unambiguously bimodal, allowing the threshold to be
184 selected at the local minimum between these two modes. When there was no evidence of bimodality a
185 value of 120ms was chosen, corresponding to the maximum value selected for the other channels. All
186 inter-spike intervals aligned to slow wave peaks with duration exceeding the threshold were considered
187 off periods. Finally, the metric termed off occupancy was defined, for each 4-second epoch, as the
188 percentage of time spent in a detected off period during that epoch. Just as with SWA (see above), the
189 median value of off occupancy over NREM sleep episodes was used to represent the level of Process S.

Model fitting and parameter optimisation

Three theoretical models were used to describe the time course of Process S (see Results). The model equations were solved using a discrete time approximation, iteratively updating the value of modelled Process S in time steps of 4 seconds (Euler method). The fitting of various models to a particular channel of data is equivalent to finding the optimal choice of parameters to achieve the closest match between simulation and empirical SWA/off occupancy. In all models, the initial value of Process S was included as an additional free parameter. The selection of parameter values for model fitting was achieved using a semi-automated approach. First, an algorithmic methodology was established, which depends primarily on the definition of an error metric to assess fit quality between modelled Process S and empirical data. For each animal, NREM sleep episodes were identified with a duration of at least 1 minute. For each NREM sleep episode ($\boldsymbol{n=1:N}$), the median empirical SWA/off occupancy ($\boldsymbol{X_n}$), and similarly the median modelled value of Process S ($\boldsymbol{S_n}$), were computed. The error metric ($\boldsymbol{E}$) is defined as the sum of absolute differences between model and data, weighted by the relative episode duration ($\boldsymbol{w_n}$). This weight was defined as the absolute duration ($\boldsymbol{d_n}$) of the NREM sleep episode in seconds, normalised by the total duration of all episodes.

$$E = \sum_{n=1:N} w_n . |X_n - S_n|$$

$$w_n = d_n / \sum_{i=1:N} d_i$$

Algorithmic parameter optimisation was performed separately for each channel, aiming to minimise this error metric. This was achieved using the Matlab function *fminsearch*, which uses the Nelder-Mead simplex algorithm (Lagarias et al., 1998). Many parameter combinations produce very similar dynamics. Therefore, there exist many possible optimal (or near-optimal) parameter regimes and so algorithmic optimisation is sensitive to initial values. For this reason, initial values for the parameters were first set manually, aided with the use of a custom-made Matlab graphical user interface. Manually selected values were then fed into the algorithmic optimisation. Final parameter values were visually inspected to ensure that this optimisation produced an improvement of fit.

The final fit quality of a model to the data was expressed as the median percent error (***E****). This is calculated by finding the absolute difference between median empirical ($\boldsymbol{X_n}$) and simulated ($\boldsymbol{S_n}$) SWA/off occupancy for each NREM sleep episode, expressed as a percentage of the empirical SWA/off occupancy in that episode. ***E**** is then defined as the median over all NREM sleep episodes of these difference values. This alternative error metric is used for presentation of results because it has more comprehensible units (percentage of empirical SWA/off occupancy) compared to the error metric, with arbitrary units.

$$E^* = \underset{n=1:N}{\text{median}}\left[\frac{|X_n - S_n|}{X_n}.100\%\right]$$

Statistical analyses

The correlation between wake duration, wake firing rates and changes in SWA was calculated separately for each LFP channel. We first identified episodes of NREM sleep of at least 1-minute duration (exactly as for modelling) and obtained the median SWA in each episode. We then identified which intervening time periods, between two NREM episodes, comprised at least 80% wake and lasted at least 5 minutes. We then calculated Pearson correlation coefficients between i) the duration of these wake periods, ii) the mean multi-unit firing rate during these periods, and iii) the change in median SWA from preceding to the following NREM sleep episode.

Analysis of variance was performed to explore factors influencing model parameters and fit quality using the Matlab functions *anova1* (one-way) and *anovan* (two-way with unequal group size). For the rate parameters, ANOVA was calculated after applying a log transform. The effect size ($\boldsymbol{\eta^2}$) is calculated for a factor as its sum of squares divided by the total sum of squares in the ANOVA and reflects the fraction of the variance accounted for by that factor.

To summarise the results in figures, boxplots were included alongside individual data points. These indicate the median, 25th and 75th percentile, with whiskers extending to the most extreme value which falls within 150% of the interquartile range of the box. For these plots, results from individual channels were typically pooled across animals. In some cases, where indicated, channels from the same animal were presented as separate populations.

Results

We selected a dataset of chronic recordings of frontal electroencephalogram (EEG) alongside local field potential (LFP) and multi-unit activity (MUA) spiking from primary motor cortex from six mice. These recordings were made continuously over 48 hours, starting at light onset, while the mice were freely behaving within their cage and exposed to a standard 12hr-12hr light-dark cycle. At light onset of the second day a sleep deprivation protocol was enforced for 6 hours, involving the presentation of novel objects. Outside of this sleep deprivation period, mice were undisturbed and able to sleep at will.

Process S dynamics can be described as a function of vigilance state history

NREM sleep can be defined and distinguished from waking by the presence of high amplitude slow (0.5 - 4Hz) waves in the EEG. The average EEG spectral power in the slow wave range (termed slow wave activity; SWA) in NREM sleep varies as a function of the animal's recent sleep-wake history, and this relationship has been captured in a classical quantitative theory using the concept of "Process S" (Borbély, 1982; Daan et al., 1984). Process S describes a variable whose magnitude can be estimated using the level of SWA during NREM sleep, reflecting the intensity of sleep, and which is interpreted as corresponding to the homeostatic component of sleep drive (Franken et al., 1991a; Achermann et al., 1993; Huber et al., 2000a; Vyazovskiy et al., 2007; Guillaumin et al., 2018). Theoretically, this Process S follows simple dynamics; during wake it increases according to a saturating exponential function towards an upper asymptote, and similarly during NREM sleep it decays exponentially towards a lower asymptote. There are many published variants of the precise equations for this model, but crucially, all these variants use the sleep-wake state history of the animal as the key predictive variable for Process S. Here, the specific equations used are:

$$\text{Wake/REM Sleep:} \quad {dS}/{dt} = \alpha(S_{max} - S(t))$$

$$\text{NREM Sleep:} \quad {dS}/{dt} = -\beta(S(t) - S_{min})$$

Where $\boldsymbol{S}$ represents the level of Process S, $\boldsymbol{S_{max}}$ and $\boldsymbol{S_{min}}$ are upper and lower asymptotes, and $\boldsymbol{\alpha}$ and $\boldsymbol{\beta}$ are rate parameters. The first equation is applied when the animal is scored to be awake or in REM sleep and the second equation is applied when it is scored to be in NREM sleep. Here, we use the typical

264 approach of applying the wake dynamics equation to REM sleep (Franken et al., 1991a; Huber et al.,
265 2000a; Vyazovskiy et al.; 2007), but for simplicity do not set separate parameters for wake vs. REM
266 sleep. For convenience, ***S*** is expressed in units equivalent to those of SWA. This classical formulism is
267 later abbreviated as model Cl-SWA. Process S as described by these simple dynamics accounts for the
268 time course of empirical SWA with high accuracy. We applied this model to SWA derived from the frontal
269 EEG of all animals, and as expected obtained a high quality fit (Figure 1A).

270 **Neuronal firing rates are associated with Process S dynamics and vigilance state distributions**

271 Whichever specific processes within the brain underpin these state-dependent dynamics for Process S,
272 it is likely associated in some way to neuronal spiking activity. Spiking patterns differ characteristically
273 between wake and NREM sleep, due to the presence of off periods in NREM sleep which typically
274 coincide with slow waves in both EEG and LFP (Figure 1B). The occurrence of such spiking off periods
275 cause firing rates to be typically much lower during NREM sleep compared to wake and REM sleep. In
276 this dataset, the mean multi-unit firing rate averaged over all periods of wake was larger than the firing
277 rate averaged over all periods of NREM sleep in every recording channel and every animal (Figure 1C).

278 Because the slow oscillation is underpinned by local neuronal dynamics, it is expected to be highly
279 heterogeneous across the neocortex. Regional differences in SWA dynamics have been previously
280 described, for example between frontal and occipital EEG derivations (Werth et al., 1996; Huber et al.,
281 2000b), and can be accounted for within the classical Process S model through the selection of locally
282 variable values for model rate parameters (Zavada et al., 2009; Rusterholz & Achermann, 2011;
283 Guillaumin et al., 2018). To explore whether spike firing rates might account for some of the variation
284 in the rate of Process S increase, we correlated the change in LFP SWA from one NREM sleep episode to
285 the next, when separated by wakefulness lasting at least 5 minutes, with the mean spike firing rate
286 during this intervening wake period, and with the duration of that wake period. Correlation coefficients
287 were obtained separately for each recording channel, and pooled across animals. As expected, we
288 obtained large positive correlation coefficients between the duration of a period of wakefulness and the
289 change in LFP SWA in all channels (mean=0.66, sd=0.13; Figure 1D). Importantly however, the change
290 in LFP SWA was on average also positively correlated with firing rate (mean=0.27, sd=0.30; Figure

291 1D,E), meaning that, generally, a higher firing rate during waking was associated with a larger increase
292 in SWA in subsequent NREM sleep. Interestingly, these phenomena were not independent, as a positive
293 correlation was also found between wake episode duration and firing rate (mean=0.35, sd= 0.33; Figure
294 1D). These results further support the possibility that neuronal activity is associated with Process S
295 dynamics and vigilance state distributions. To test this hypothesis we next turned to a quantitative
296 modelling approach.

297 **Process S dynamics can be described as a function of neuronal firing rates**

298 We first sought to determine whether a model expressing Process S dynamics solely as a function of
299 local multi-unit neuronal firing rates might describe the levels of sleep SWA in the corresponding LFP
300 with comparable accuracy to the classical model dependent on vigilance states at the global level. The
301 classical Process S model was used as a starting point for the development of a novel firing rate
302 dependent alternative. To do this, the equations of the classical model were adapted in two ways. Firstly,
303 an instantaneous firing rate threshold ($\boldsymbol{F_\theta}$) was introduced as a new model parameter to replace the
304 wake vs. sleep criterion, assuming an increase in Process S when the threshold is exceeded and decrease
305 when firing is below. Conceptually, this firing rate threshold resembles a set point; a target firing rate at
306 which the dynamics are stable. Secondly, we assumed that the rate of change of Process S is proportional
307 to the difference between firing rate and this threshold. Introducing this change to the equations ensures
308 that the rate of change of $\boldsymbol{S}$ is equal to zero exactly at the set point, and a continuous function of firing
309 rate around this value. This version of the model is later abbreviated as Fr-SWA. The equations are:

$$F(t) > F_\theta: \quad {dS}/{dt} = \alpha(S_{max} - S(t))(F(t) - F_\theta)$$

$$F(t) < F_\theta: \quad {dS}/{dt} = -\beta(S(t) - S_{min})(F_\theta - F(t))$$

$$F(t) = F_\theta: \quad {dS}/{dt} = 0$$

310 We applied this novel model, alongside the classical model, to describe SWA dynamics at the LFP level,
311 by finding parameter values that would minimise the difference between empirical SWA and modelled
312 Process S. The two models were fit to the SWA from each LFP channel separately, using the multi-unit
313 firing rate from the same channel for the firing-rate-dependent model. The models were also fit to the

SWA obtained by averaging the LFP (and firing rate) over the whole population of channels within the same mouse.

Figure 2 shows two examples of the fit of both models, first to SWA derived from the average LFP, and also to SWA derived from a single LFP channel (these examples are from the same animal as in Figure 1A). The overall pattern of Process S dynamics is similar at both recording levels, and to the corresponding EEG, and is well described by both the classic and novel firing-rate-based model. Throughout the dataset, this purely firing-rate-dependent model described the overall dynamics of LFP SWA during NREM sleep to a comparable accuracy as the classical model, as reflected in the median percent error deviation between modelled and empirical SWA (Figure 3B). Both the model type and animal have a highly significant effect on the median percent error of the model fit to individual LFP channels, although there is no significant interaction (Model: $F_{(1, 144)} = 25.9$, $p = 1.1\text{x}10^{-6}$; Animal: $F_{(5, 144)} = 30.2$, $p = 6.3\text{x}10^{-21}$; Model x Animal: $F_{(5, 144)} = 1.65$, $p = 0.15$; two-way ANOVA unequal groups). Errors were higher for the novel model, importantly however, the differences in fit quality due to the model type are small relative to the effect size of the particular animal and channel, on which fit quality depends much more strongly (Model: $\eta^2 = 0.079$; Animal: $\eta^2 = 0.459$; Model x Animal: $\eta^2 = 0.025$; Channel (residuals): $\eta^2 = 0.437$). The errors of the model fit on the averaged LFP and on the EEG (classical model only) are also shown in Figure 3B, and are more explicitly compared in Figure 3C. We do not find any significant effect of the field potential level (EEG, average LFP, single LFP) on the model error ($F_{(2,171)} = 0.2$, $p = 0.82$, one-way ANOVA).

The distributions of final optimised parameters are shown in Figure 3D-G for the classic model and Figure 3H-L for the firing rate based model. Most parameters in both models were significantly different between animals, with the exception of $\boldsymbol{S_{min}}$ in the firing rate dependent model (Cl-SWA $\boldsymbol{\alpha}$: $F_{(5,77)} = 4.03$, $p = 2.8\text{x}10^{-3}$; Cl-SWA $\boldsymbol{\beta}$: $F_{(5,77)} = 8.65$, $p = 1.9\text{x}10^{-6}$; Cl-SWA $\boldsymbol{S_{max}}$: $F_{(5,77)} = 14.35$, $p = 9.8\text{x}10^{-10}$; Cl-SWA $\boldsymbol{S_{min}}$: $F_{(5,77)} = 12.42$, $p = 1.1\text{x}10^{-8}$; Fr-SWA $\boldsymbol{\alpha}$: $F_{(5,77)} = 8.33$, $p = 3.0\text{x}10^{-6}$; Fr-SWA $\boldsymbol{\beta}$: $F_{(5,77)} = 9.27$, $p = 7.5\text{x}10^{-7}$; Fr-SWA $\boldsymbol{F_\theta}$: $F_{(5,77)} = 14.3$, $p = 1.0\text{x}10^{-9}$; Fr-SWA $\boldsymbol{S_{max}}$: $F_{(5,77)} = 6.64$, $p = 3.9\text{x}10^{-5}$; Fr-SWA $\boldsymbol{S_{min}}$: $F_{(5,77)} = 2.16$, $p = 0.07$; one way ANOVA). The optimised rate parameters for EEG and averaged LFP data consistently fall within the range of the single channel population (Figure 3D-L). The relationship between the optimal

341 firing set point and state specific firing rates is shown in Figure 3M. Firing rate threshold was z-
342 normalised (subtract mean, divide by standard deviation) separately with respect to the distribution of
343 firing rates in wake, NREM and REM sleep. This shows, as expected, that the set point is typically below
344 mean firing in wake (-1.0 ± 0.6; mean ± sd), well above mean firing in NREM sleep (1.6 ± 1.1), and slightly
345 above mean firing of REM sleep (0.7 ± 1.1). These were all significantly different from zero (wake: $p = 1.6x10^{-13}$, NREM: $p = 1.9x10^{-14}$, REM: $p = 3.4x10^{-7}$, two-sided Wilcoxon signed rank test). Figure 3N
347 further shows the state dependent distribution of average firing rate, expressed as a percentage of the
348 chosen firing set point parameter. Mean firing was 182 ± 57.6% of the firing rate set point during wake,
349 61.8 ± 17.6 % during NREM sleep, and 84.2 ± 31.8 % during REM sleep. Again, these distributions were
350 all significantly different from 100% (Wake: $p = 6.7x10^{-14}$, NREM: $p = 2.0x10^{-14}$, REM: $p = 5.4x10^{-5}$). Note
351 that, in a few channels, the optimal firing rate threshold is actually above the mean firing rate during
352 waking. This occurs when the waking firing rate distribution overlaps substantially with the NREM sleep
353 firing rate distribution but has a heavier tail. REM sleep, in this dataset, is typically associated with firing
354 below the set point, and therefore Process S decrease, albeit at a reduced rate compared to NREM sleep
355 (Figure 3O). Interestingly, there are no significant correlations between the model fit error and the
356 threshold normalisation relative to any one vigilance state (Wake: p=0.06, r=0.21; NREM: p=0.35, r=-
357 0.11; REM: p=0.94, r=-0.01), suggesting that there is no clear relationship between the firing rate set
358 point and firing rate distribution of any one particular state.

359 **Process S can be defined in terms of neuronal spiking off periods**

360 When considering the relationship between multi-unit firing rates and LFP slow waves, a conceptual
361 complication arises due to the different origins of the LFP and MUA from within the same channel. While
362 the MUA firing rate represents the activity of only a few individual neurones, factors such as volume
363 conduction result in spatial smoothing of the LFP signal, and as such it represents the combined activity
364 of neurones covering a cortical area potentially on the order of several millimetres (Kajikawa &
365 Schroeder, 2011). This means that when a slow wave is detected in the LFP, it is not guaranteed that
366 local neurones which contribute to the MUA are necessarily in an off period. Similarly, not every long
367 interspike interval occurs during a slow wave. An estimation of the occurrence of off periods may be

368 obtained by combining LFP and spiking data (Figure 4A). Slow wave detection was performed on each
369 LFP over the whole 48hrs, including all vigilance states (0.5-6 Hz filter followed by an amplitude
370 threshold, values shown in Figure 4C). All multi-unit inter-spike intervals (ISIs) which coincide with the
371 peak of detected slow waves were identified. The distribution of the duration of these ISIs was often (64
372 out of 75 channels) unambiguously bimodal (Figure 4B). This could be interpreted as evidence of the
373 existence of two spiking states occurring locally during the more widespread network slow oscillation;
374 high frequency spiking (on period) and extended silence (off period). Note that these two distributions
375 do not simply correspond exactly to sleep vs. wake conditions, because bimodality is often evident in
376 the distribution of slow wave coincident ISIs from NREM sleep only, or even from REM sleep only (Figure
377 4B). The distribution of slow wave coincident ISIs (over all vigilance states) was used to define an ISI
378 duration threshold for the detection of off periods, separately for each channel. The values used for this
379 threshold are shown in Figure 4D. The average multi-unit firing rate aligned to the peak of slow waves
380 in detected off periods reveals a clear suppression of firing, consistent with expectations (Figure 4E). A
381 rebound increase in average firing is visible in this example channel immediately after the off period, as
382 has been previously documented in some cortical neuronal populations (Chauvette et al., 2010). The
383 total fraction of time each channel spends in off periods was calculated over all 4-second epochs, and
384 termed the "off occupancy". Off occupancy defined in this way is high in NREM sleep and low in both
385 wake and REM sleep (Figure 4F). The existence of a non-zero frequency of local cortical off periods has
386 been previously reported during wakefulness (Vyazovskiy et al., 2011; Vyazovskiy et al., 2014; Fisher et
387 al., 2016), and REM sleep (Funk et al., 2016). The off occupancy measure displays similar temporal
388 dynamics to LFP (and EEG) SWA over both sleep deprivation and spontaneous sleep and wake (Figure
389 4G).

390 **Process S dynamics, defined using off periods, can be described as a function of vigilance states**
391 **or neuronal firing rates**

392 In order to investigate whether the off occupancy measure reflects Process S, we applied the classical
393 state based model to the time course of off occupancy, exactly as was done with single channel SWA. The
394 classical model was applied with its equations unchanged, and is abbreviated as Cl-Off. Figure 5A shows

395 an example of the resulting Process S time course obtained in this way with a high quality of fit. In
396 contrast, some changes were introduced to the firing-rate-based model in order to describe off
397 occupancy dynamics. We considered that the different dynamics above vs. below a particular firing rate
398 set point may be due to two opponent processes simultaneously active in dynamic opposition but with
399 differential magnitude in wake vs. NREM sleep. Specifically, we consider a Process S increasing term
400 which is proportional to instantaneous firing rate, and a Process S decreasing term which is proportional
401 to the time spent in off periods (off occupancy). The equation used is:

402 $$dS/dt = \alpha F(t)\big(S_{max} - S(t)\big) - \beta X(t)(S(t) - S_{min})$$

403 In this model, one term drives $\boldsymbol{S}$ towards an upper asymptote ($\boldsymbol{S_{max}}$) in proportion to firing rate ($\boldsymbol{F}$), while
404 the other drives $\boldsymbol{S}$ towards a lower asymptote ($\boldsymbol{S_{min}}$) in proportion to the off occupancy ($\boldsymbol{X}$). Again, two
405 rate parameters $\boldsymbol{\alpha}$ & $\boldsymbol{\beta}$ are required. This model behaves similarly to previous models because firing is
406 high in wake and low in NREM sleep, whereas off occupancy is high in NREM sleep and low in wake. This
407 variant of the model is abbreviated as Fr-Off. Figure 5A includes also the fit from this model,
408 demonstrating a high level of agreement between the two models and an accurate fit to the data.

409 The distribution over all animals and channels of the median percent errors for the fits from both models
410 is shown in Figure 5C. As before, the model type and animal has a significant effect (Model: $F_{(1,138)} = 8.06$,
411 $p = 5.2\text{x}10^{-3}$; Animal: $F_{(5,138)} = 17.2$, $p = 3.2\text{x}10^{-13}$; Model x Animal: $F_{(5,138)} = 0.52$, $p = 0.76$; two-way ANOVA
412 with unequal groups) and the classic model achieved a slightly lower median percent error. However,
413 this effect was again very weak compared with the variation in fit quality between animals and channels
414 (Model: $\eta^2 = 0.034$; Animal: $\eta^2 = 0.367$; Model x Animal: $\eta^2 = 0.011$; Channel (residuals): $\eta^2 = 0.588$).
415 Figure 5D shows the distribution of values for the change in modelled Process S from one time step to
416 the next resulting from the firing-rate-based model (Fr-Off), in wake, NREM sleep and REM, pooling all
417 animals, channels and time. Unlike in the previous firing-rate-based model, REM sleep is now typically
418 associated with Process S increase. The distributions of final optimised parameters are shown in Figure
419 5E-H for the classic model and Figure 5I-L for the firing rate and off occupancy model. Most parameters
420 in both models were different between animals to a high significance level (Cl-Off $\boldsymbol{\alpha}$: $F_{(5,74)} = 2.4$, $p =$
421 0.047; Cl-Off $\boldsymbol{\beta}$: $F_{(5,74)} = 2.29$, $p = 0.055$; Cl-Off $\boldsymbol{S_{max}}$: $F_{(5,74)} = 9.49$, $p = 6.4\text{x}10^{-7}$; Cl-Off $\boldsymbol{S_{min}}$: $F_{(5,74)} = 16.79$, p

422 = 8.0×10^{-11}; Fr-Off $\boldsymbol{\alpha}$: $F_{(5,74)} = 9.86$, $p = 3.9 \times 10^{-7}$; Fr-Off $\boldsymbol{\beta}$: $F_{(5,74)} = 5.14$, $p = 4.6 \times 10^{-4}$; Fr-Off $\boldsymbol{S_{max}}$: $F_{(5,74)} =$

423 10.08, $p = 2.8 \times 10^{-7}$; Fr-Off $\boldsymbol{S_{min}}$: $F_{(5,74)} = 10.25$, $p = 2.3 \times 10^{-7}$; one way ANOVA). Notably, the weakest

424 evidence for inter-animal differences were for $\boldsymbol{\alpha}$ and $\boldsymbol{\beta}$ in the classic model.

425 **Modelling identifies local variation in Process S dynamics**

426 All four modelling approaches described here suggest the existence of variability in Process S between

427 recording channels, indicating that a local component determines its dynamics. Figure 6A-D illustrates

428 this diversity, showing the overlaid time courses of Process S for all channels within a single

429 representative animal, expressed as a percentage of their individual maximum value for normalisation

430 purposes. Although the models all fit empirical SWA or off period occupancy with generally high

431 accuracy, there are nonetheless differences between models in the precise shape of Process S. The

432 average Process S over all channels was also calculated for each model and compared with the Process

433 S derived from applying the classical model to EEG SWA (Figure 6E). This reveals that Process S derived

434 from modelling LFP SWA more closely resembles Process S derived from EEG SWA than Process S

435 derived from off occupancy. This suggests that global Process S calculated at a higher spatial scale might

436 reflect an averaging across a manifold of local Processes S that exist on a finer spatial level.

Discussion

Here, we show that Process S can be quantitatively described entirely in terms of measures based on neuronal spiking activity, without reference to global vigilance states. A model was outlined whereby the integrated history of multi-unit firing rates, relative to a firing rate set point, predicted the temporal dynamics of LFP SWA. The accuracy of this model was demonstrated in a dataset of recordings from mouse frontal cortex over 48 hours, including both voluntary sleep and wake, and sleep deprivation. A novel metric for Process S was then presented, termed off occupancy, which measures the fraction of time a neural population spends in off periods, defined by the coincidence of LFP slow waves and multi-unit spiking silence. The modelling approach was combined with the off occupancy metric and tested on the same dataset to present a quantitative framework for understanding dynamics of sleep pressure at a highly local level in terms of neural spiking and off periods.

Central to this modelling perspective is the assumption that the generation of spikes by a neural network is in some way correlated with an increase in sleep pressure, and that this manifests in the subsequent expression of slow waves and off periods, reflecting Process S. The energetic cost of spiking is high (Attwell & Laughlin 2001), the regulation of a neurone's firing rate set point is linked to cellular energetics (Styr et al., 2019; Vergara et al., 2019), and neurones are susceptible to cellular stresses that can result from sustained metabolic load, such as oxidative stress (Wang & Michaelis 2010; Cobley et al., 2018; Kempf et al., 2019). Furthermore, spiking activity may be mechanistically associated with synaptic plasticity, and it was suggested that firing rates are an important determinant of overall changes in synaptic strength, with higher spiking leading to greater changes (Graupner et al., 2016; Lappalainen et al., 2019). Compensatory processes exist within neurones to oppose cellular stress and related homeostatic challenges (Kültz 2005) and off periods could provide the opportunity for neurones to prioritise such processes, therefore mediating the restorative benefits of sleep (Vyazovskiy & Harris, 2013). Similarly, off periods are associated with distinct synaptic plasticity rules (Gonzalez-Rueda et al., 2018), and so their prevalence and patterning is likely also related to whatever regulation of synaptic strength occurs during sleep (Tononi & Cirelli 2014; Timofeev & Chauvette 2017; Seibt & Frank, 2019).

463 According to this view of sleep homeostasis, in principle, regulation can occur entirely at the local level,
464 within cortical networks or perhaps even single neurones. Indeed, this is reflected in our results through
465 the differences between channels both with respect to the accuracy of the model and in the values of
466 optimised parameters. Why then is global sleep preferred over a hypothetical state including
467 asynchronous local off periods, which presumably could be used to sustain longer periods of
468 behavioural wakefulness? It has been argued previously that it is ecologically optimal to synchronise off
469 periods and undergo dedicated periods of total behavioural shutdown, because local off periods during
470 waking impair behaviour (Vyazovskiy et al., 2011; Rattenborg et al., 2012). Mechanistically, the
471 occurrence of off periods might be obstructed by strong synaptic coupling and shared neuromodulatory
472 tone. Indeed, it has been observed that the degree of coupling between an individual neurone's firing
473 and the population firing rate, is variable between cells but characteristic to an individual neurone and
474 likely reflects total synaptic strength with its neighbours (Okun et al., 2015). Some neurones may
475 therefore be less able to express asynchronous off periods than others.

476 The preference for global sleep, despite its fundamentally local mechanisms, may be evidence that sleep
477 homeostasis ultimately does not serve a single specific local function. Instead, the recent history of local
478 activities, by alteration of the local propensity to generate off periods (Process S), may be integrated
479 over neuronal populations through intrinsic network mechanisms, in order to produce a sleep
480 propensity signal that estimates the total time spent awake with great accuracy. The brain would
481 thereby aim to enforce a daily quota of sleep, which could have many physiological and ecological
482 benefits, rather than initiating sleep in response to the homeostatic need of one specific regulated
483 variable (Vyazovskiy, 2015). The overall accuracy of both firing-rate-based and vigilance-state-based
484 models supports this possibility, as does the evidence that homeostatically regulated cellular variables
485 can actually be stable during extended wakefulness and that maintenance processes in sleep are
486 ultimately prophylactic (Vyazovskiy & Harris, 2013). In this case, the sleep quota typically required by
487 the brain would be determined by the neural population(s) that regularly accumulate sleep pressure
488 the fastest. In order to maximise the efficiency of global sleep, single neuronal activities may be
489 modulated such that sleep pressure accumulates, on average, as uniformly as possible. This is consistent
490 with recent reports that sleep regulates the population level firing rate distribution (Watson et al., 2016;

491 Levenstein et al., 2017; Miyawaki & Diba, 2019) and could account for sleep's link with synaptic and
492 firing rate homeostasis, reconciling the local origins of sleep pressure accumulation with the global level
493 of its dissipation.

494 Here, spike firing rate is used to represent the level of neural activity because it is convenient to record,
495 locally variable, and directly linked to neuronal functionality. However, no strong claim is made that
496 firing rates are necessarily causally responsible for the accumulation of sleep pressure. Indeed, it would
497 likely be possible to obtain a reasonable quantitative account of sleep homeostasis using any
498 physiological variable (or set of variables) that are consistently higher in either the wake or sleep state.
499 For example, a model assuming that Process S increases in proportion to local cortical temperature,
500 which drops by ~2°C when falling asleep (Franken et al., 1991b) and which has been mechanistically
501 implicated in sleep regulation (Hoekstra et al., 2019), might also provide a plausible description of
502 Process S dynamics. Importantly, these results demonstrate that firing rates are a useful measurable
503 correlate of the processes that directly underpin Process S, and therefore firing rate variance resulting
504 from differences in experience and behaviour may well account for the variance in Process S
505 accumulation in normal individuals, between waking periods and between cortical regions.

506 It should be addressed explicitly that the novel firing rate based models typically slightly under-perform,
507 relative to the classic model, in terms of minimising the error between simulation and empirical data.
508 There are a number of reasons why a limit on the accuracy of the model is to be expected, related to
509 technical restrictions rather than conceptual ones. In this approach, each MUA channel records only a
510 few randomly sampled nearby neurones, which may have very different spiking properties, and so
511 grouping these as a single measure of local network activity is somewhat artificial. It may be valuable to
512 explore genetic and pharmacological manipulations of firing rate in order to further test this model's
513 validity. Unfortunately, the effects of any manipulation on the accumulation, expression and dissipation
514 of sleep pressure, separately to the effects on firing, is unknown, and so this may be hard to interpret.
515 For example, a recent study found that systemic atropine administered during behavioural wakefulness
516 produces slow wave activity, reducing spiking (as measured by c-Fos) yet increasing the duration of
517 subsequent NREM sleep (Qiu et al., 2015). While this was interpreted as evidence that spiking activity

518 is not related to sleep pressure accumulation, the direct effects of atropine on Process S and the
519 functional significance of the resulting induced slow oscillation are unclear. Similarly, another study
520 found that optogenetic activation of cortex during sleep, despite raising firing rates to waking levels,
521 was accompanied with decreased Process S (lower SWA and fewer off periods) during subsequent
522 NREM sleep (Rodriguez et al., 2016). Again, it is difficult to disentangle the direct effects of this
523 stimulation, which is not physiologically realistic, on the mechanisms surrounding the accumulation,
524 expression and dissipation of sleep pressure. On the other hand, these results might be interpreted as
525 evidence that the expression of the level of Process S involves an integration of homeostatic sleep need
526 across neural populations and therefore local firing rate manipulations are not able to substantially
527 influence Process S dynamics at a global level.

528 It is reasonable to assume that sleep homeostasis unfolds on multiple time scales and Process S as
529 defined by these models describes a relatively fast one, approaching its upper asymptote after
530 continuous wakefulness on a time scale of hours. The inclusion of processes acting over longer or
531 shorter time scales might explain discrepancies in all these models, however, the challenge remains to
532 identify what these could be. Furthermore, the role of REM sleep in Process S dynamics has not been
533 explicitly addressed or considered in the construction of these models. Depending on the model variant,
534 REM sleep is associated either with small increase or small decrease in Process S, because firing rates
535 are low in REM sleep (closer to NREM sleep than waking) and yet off period occupancy is also low (closer
536 to wake levels than NREM sleep). It is possible that REM sleep might represent a homeostatically neutral
537 state, in which the level of Process S changes little, or not at all (Vyazovskiy & Delogu, 2014).

538 In summary, Process S is reflected in both slow wave activity and the occurrence of local off periods, and
539 its dynamics can be quantitatively described using information derived from local spike firing rates and
540 off periods. Such a description has comparable accuracy to the classical model of Process S, dependent
541 only on global sleep-wake history. This result has important implications for our understanding of the
542 nature of sleep homeostasis and these novel models provide a methodology to quantify and compare
543 Process S dynamics, potentially between different cell types and brain regions.

References

Achermann, P., Dijk, D.-J., Brunner, D.P., and Borbély, A.A. (1993). A model of human sleep homeostasis based on EEG slow-wave activity: Quantitative comparison of data and simulations. Brain Research Bulletin *31*, 97–113.

Attwell, D., and Laughlin, S.B. (2001). An energy budget for signaling in the grey matter of the brain. J. Cereb. Blood Flow Metab. *21*, 1133–1145.

Bellesi, M., Bushey, D., Chini, M., Tononi, G., and Cirelli, C. (2016). Contribution of sleep to the repair of neuronal DNA double-strand breaks: evidence from flies and mice. Scientific Reports *6*, 36804.

Borbély, A.A. (1982). A two process model of sleep regulation. Hum Neurobiol *1*, 195–204.

Bukhtiyarova, O., Soltani, S., Chauvette, S., and Timofeev, I. (2019). Slow wave detection in sleeping mice: Comparison of traditional and machine learning methods. Journal of Neuroscience Methods *316*, 35–45.

Buzsáki, G., Anastassiou, C.A., and Koch, C. (2012). The origin of extracellular fields and currents — EEG, ECoG, LFP and spikes. Nature Reviews Neuroscience *13*, 407–420.

Chauvette, S., Volgushev, M., and Timofeev, I. (2010). Origin of Active States in Local Neocortical Networks during Slow Sleep Oscillation. Cereb Cortex *20*, 2660–2674.

Cirelli, C., Faraguna, U., and Tononi, G. (2006). Changes in brain gene expression after long-term sleep deprivation. Journal of Neurochemistry *98*, 1632–1645.

Cobley, J.N., Fiorello, M.L., and Bailey, D.M. (2018). 13 reasons why the brain is susceptible to oxidative stress. Redox Biology *15*, 490–503.

Daan, S., Beersma, D.G., and Borbély, A.A. (1984). Timing of human sleep: recovery process gated by a circadian pacemaker. Am. J. Physiol. *246*, R161-183.

Fisher, S.P., Cui, N., McKillop, L.E., Gemignani, J., Bannerman, D.M., Oliver, P.L., Peirson, S.N., and Vyazovskiy, V.V. (2016). Stereotypic wheel running decreases cortical activity in mice. Nature Communications *7*, ncomms13138.

569 Frank, M.G., and Heller, H.C. (2019). The Function(s) of Sleep. Handb Exp Pharmacol.

570 Franken, P., Dijk, D.J., Tobler, I., and Borbély, A.A. (1991a). Sleep deprivation in rats: effects on EEG
571 power spectra, vigilance states, and cortical temperature. American Journal of Physiology-Regulatory,
572 Integrative and Comparative Physiology *261*, R198–R208.

573 Franken, P., Tobler, I., and Borbély, A.A. (1991b). Sleep homeostasis in the rat: simulation of the time
574 course of EEG slow-wave activity. Neurosci. Lett. *130*, 141–144.

575 Funk, C.M., Honjoh, S., Rodriguez, A.V., Cirelli, C., and Tononi, G. (2016). Local Slow Waves in Superficial
576 Layers of Primary Cortical Areas during REM Sleep. Curr. Biol. *26*, 396–403.

577 González-Rueda, A., Pedrosa, V., Feord, R.C., Clopath, C., and Paulsen, O. (2018). Activity-Dependent
578 Downscaling of Subthreshold Synaptic Inputs during Slow-Wave-Sleep-like Activity In Vivo. Neuron
579 *97*, 1244-1252.e5.

580 Graupner, M., Wallisch, P., and Ostojic, S. (2016). Natural Firing Patterns Imply Low Sensitivity of
581 Synaptic Plasticity to Spike Timing Compared with Firing Rate. J Neurosci *36*, 11238–11258.

582 Grosmark, A.D., Mizuseki, K., Pastalkova, E., Diba, K., and Buzsáki, G. (2012). REM Sleep Reorganizes
583 Hippocampal Excitability. Neuron *75*, 1001–1007.

584 Guillaumin, M.C.C., McKillop, L.E., Cui, N., Fisher, S.P., Foster, R.G., de Vos, M., Peirson, S.N., Achermann,
585 P., and Vyazovskiy, V.V. (2018). Cortical region specific sleep homeostasis in mice: effects of time of
586 day and waking experience. Sleep.

587 Hengen, K.B., Lambo, M.E., Van Hooser, S.D., Katz, D.B., and Turrigiano, G.G. (2013). Firing Rate
588 Homeostasis in Visual Cortex of Freely Behaving Rodents. Neuron *80*, 335–342.

589 Hengen, K.B., Pacheco, A.T., McGregor, J.N., Van Hooser, S.D., and Turrigiano, G.G. (2016). Neuronal
590 firing rate homeostasis is inhibited by sleep and promoted by wake. Cell *165*, 180–191.

591 Hoekstra, M.M., Emmenegger, Y., Hubbard, J., and Franken, P. (2019). Cold-inducible RNA-binding
592 protein (CIRBP) adjusts clock-gene expression and REM-sleep recovery following sleep deprivation.
593 ELife *8*.

Huber, R., Deboer, T., and Tobler, I. (2000a). Effects of sleep deprivation on sleep and sleep EEG in three mouse strains: empirical data and simulations. Brain Res. *857*, 8–19.

Huber, R., Deboer, T., and Tobler, I. (2000b). Topography of EEG dynamics after sleep deprivation in mice. J. Neurophysiol. *84*, 1888–1893.

Huber, R., Ghilardi, M.F., Massimini, M., and Tononi, G. (2004). Local sleep and learning. Nature *430*, 78–81.

Kajikawa, Y., and Schroeder, C.E. (2011). How local is the local field potential? Neuron *72*, 847–858.

Kempf, A., Song, S.M., Talbot, C.B., and Miesenböck, G. (2019). A potassium channel β-subunit couples mitochondrial electron transport to sleep. Nature *568*, 230–234.

Krueger, J.M., and Tononi, G. (2011). Local Use-Dependent Sleep; Synthesis of the New Paradigm. Curr Top Med Chem *11*, 2490–2492.

Krueger, J.M., Rector, D.M., Roy, S., Dongen, H.P.A.V., Belenky, G., and Panksepp, J. (2008). Sleep as a fundamental property of neuronal assemblies. Nature Reviews Neuroscience *9*, 910.

Kültz, D. (2005). Molecular and Evolutionary Basis of the Cellular Stress Response. Annual Review of Physiology *67*, 225–257.

Lagarias, J., Reeds, J., Wright, M., and Wright, P. (1998). Convergence Properties of the Nelder--Mead Simplex Method in Low Dimensions. SIAM J. Optim. *9*, 112–147.

Lappalainen, J., Herpich, J., and Tetzlaff, C. (2019). A Theoretical Framework to Derive Simple, Firing-Rate-Dependent Mathematical Models of Synaptic Plasticity. Front. Comput. Neurosci. *13*.

Levenstein, D., Watson, B.O., Rinzel, J., and Buzsáki, G. (2017). Sleep regulation of the distribution of cortical firing rates. Current Opinion in Neurobiology *44*, 34–42.

Liu, Z.-W., Faraguna, U., Cirelli, C., Tononi, G., and Gao, X.-B. (2010). Direct evidence for wake-related increases and sleep-related decreases in synaptic strength in rodent cortex. J. Neurosci. *30*, 8671–8675.

618 Mackiewicz, M., Shockley, K.R., Romer, M.A., Galante, R.J., Zimmerman, J.E., Naidoo, N., Baldwin, D.A.,
619 Jensen, S.T., Churchill, G.A., and Pack, A.I. (2007). Macromolecule biosynthesis: a key function of sleep.
620 Physiol. Genomics *31*, 441–457.

621 Massimini, M., Huber, R., Ferrarelli, F., Hill, S., and Tononi, G. (2004). The sleep slow oscillation as a
622 traveling wave. J. Neurosci. *24*, 6862–6870.

623 McKillop, L.E., Fisher, S.P., Cui, N., Peirson, S.N., Foster, R.G., Wafford, K.A., and Vyazovskiy, V.V. (2018).
624 Effects of Aging on Cortical Neural Dynamics and Local Sleep Homeostasis in Mice. J. Neurosci. *38*,
625 3911–3928.

626 Miyawaki, H., and Diba, K. (2016). Regulation of hippocampal firing by network oscillations during
627 sleep. Curr Biol *26*, 893–902.

628 Miyawaki, H., Watson, B.O., and Diba, K. (2019). Neuronal firing rates diverge during REM and
629 homogenize during non-REM. Scientific Reports *9*, 689.

630 Murphy, M., Huber, R., Esser, S., Riedner, B.A., Massimini, M., Ferrarelli, F., Ghilardi, M.F., and Tononi, G.
631 (2011). The cortical topography of local sleep. Curr Top Med Chem *11*, 2438–2446.

632 Okun, M., Steinmetz, N.A., Cossell, L., Iacaruso, M.F., Ko, H., Barthó, P., Moore, T., Hofer, S.B., Mrsic-
633 Flogel, T.D., Carandini, M., et al. (2015). Diverse coupling of neurons to populations in sensory cortex.
634 Nature *521*, 511–515.

635 O'Leary, T., Williams, A.H., Franci, A., and Marder, E. (2014). Cell types, network homeostasis, and
636 pathological compensation from a biologically plausible ion channel expression model. Neuron *82*,
637 809–821.

638 Qiu, M.-H., Chen, M.C., and Lu, J. (2015). Cortical neuronal activity does not regulate sleep homeostasis.
639 Neuroscience *297*, 211–218.

640 Quiroga, R.Q., Nadasdy, Z., and Ben-Shaul, Y. (2004). Unsupervised spike detection and sorting with
641 wavelets and superparamagnetic clustering. Neural Comput *16*, 1661–1687.

Rattenborg, N.C., Lima, S.L., and Lesku, J.A. (2012). Sleep Locally, Act Globally. Neuroscientist *18*, 533–546.

Rector, D.M., Schei, J.L., Van Dongen, H.P.A., Belenky, G., and Krueger, J.M. (2009). Physiological Markers of Local Sleep. Eur J Neurosci *29*, 1771–1778.

Reimund, E. (1994). The free radical flux theory of sleep. Medical Hypotheses *43*, 231–233.

Rodriguez, A.V., Funk, C.M., Vyazovskiy, V.V., Nir, Y., Tononi, G., and Cirelli, C. (2016). Why Does Sleep Slow-Wave Activity Increase After Extended Wake? Assessing the Effects of Increased Cortical Firing During Wake and Sleep. J. Neurosci. *36*, 12436–12447.

Rusterholz, T., and Achermann, P. (2011). Topographical aspects in the dynamics of sleep homeostasis in young men: individual patterns. BMC Neurosci *12*, 84.

Saberi-Moghadam, S., Simi, A., Setareh, H., Mikhail, C., and Tafti, M. (2018). In vitro Cortical Network Firing is Homeostatically Regulated: A Model for Sleep Regulation. Sci Rep *8*, 6297.

Sanchez-Vives, M., and Mattia, M. (2014). Slow wave activity as the default mode of the cerebral cortex. Archives Italiennes de Biologie *152*, 147–155.

Scharf, M.T., Naidoo, N., Zimmerman, J.E., and Pack, A.I. (2008). The energy hypothesis of sleep revisited. Prog. Neurobiol. *86*, 264–280.

Seibt, J., and Frank, M.G. (2019). Primed to Sleep: The Dynamics of Synaptic Plasticity Across Brain States. Front Syst Neurosci *13*, 2.

Slomowitz, E., Styr, B., Vertkin, I., Milshtein-Parush, H., Nelken, I., Slutsky, M., and Slutsky, I. (2015). Interplay between population firing stability and single neuron dynamics in hippocampal networks. Elife *4*.

Steriade, M., Nuñez, A., and Amzica, F. (1993a). A novel slow (< 1 Hz) oscillation of neocortical neurons in vivo: depolarizing and hyperpolarizing components. J. Neurosci. *13*, 3252–3265.

Steriade, M., Nuñez, A., and Amzica, F. (1993b). Intracellular analysis of relations between the slow (< 1 Hz) neocortical oscillation and other sleep rhythms of the electroencephalogram. J. Neurosci. *13*, 3266–3283.

Steriade, M., Timofeev, I., and Grenier, F. (2001). Natural waking and sleep states: a view from inside neocortical neurons. J. Neurophysiol. *85*, 1969–1985.

Styr, B., Gonen, N., Zarhin, D., Ruggiero, A., Atsmon, R., Gazit, N., Braun, G., Frere, S., Vertkin, I., Shapira, I., et al. (2019). Mitochondrial Regulation of the Hippocampal Firing Rate Set Point and Seizure Susceptibility. Neuron *102*, 1009-1024.e8.

Timofeev, I., and Chauvette, S. (2017). Sleep slow oscillation and plasticity. Curr. Opin. Neurobiol. *44*, 116–126.

Tononi, G., and Cirelli, C. (2003). Sleep and synaptic homeostasis: a hypothesis. Brain Research Bulletin *62*, 143–150.

Tononi, G., and Cirelli, C. (2014). Sleep and the Price of Plasticity: From Synaptic and Cellular Homeostasis to Memory Consolidation and Integration. Neuron *81*, 12–34.

Turrigiano, G. (2011). Too Many Cooks? Intrinsic and Synaptic Homeostatic Mechanisms in Cortical Circuit Refinement. Annual Review of Neuroscience *34*, 89–103.

Vergara, R.C., Jaramillo-Riveri, S., Luarte, A., Moënne-Loccoz, C., Fuentes, R., Couve, A., and Maldonado, P.E. (2019). The Energy Homeostasis Principle: Neuronal Energy Regulation Drives Local Network Dynamics Generating Behavior. Front Comput Neurosci *13*, 49.

Vyazovskiy, V.V. (2015). Sleep, recovery, and metaregulation: explaining the benefits of sleep. Nat Sci Sleep *7*, 171–184.

Vyazovskiy, V.V., and Delogu, A. (2014). NREM and REM Sleep: Complementary Roles in Recovery after Wakefulness. Neuroscientist *20*, 203–219.

Vyazovskiy, V.V., and Harris, K.D. (2013). Sleep and the single neuron: the role of global slow oscillations in individual cell rest. Nat Rev Neurosci *14*, 443–451.

690 Vyazovskiy, V.V., and Tobler, I. (2008). Handedness leads to interhemispheric EEG asymmetry during
691 sleep in the rat. J. Neurophysiol. *99*, 969–975.

692 Vyazovskiy, V.V., Achermann, P., and Tobler, I. (2007). Sleep homeostasis in the rat in the light and
693 dark period. Brain Res. Bull. *74*, 37–44.

694 Vyazovskiy, V.V., Cirelli, C., Pfister-Genskow, M., Faraguna, U., and Tononi, G. (2008). Molecular and
695 electrophysiological evidence for net synaptic potentiation in wake and depression in sleep. Nat
696 Neurosci *11*, 200–208.

697 Vyazovskiy, V.V., Olcese, U., Lazimy, Y.M., Faraguna, U., Esser, S.K., Williams, J.C., Cirelli, C., and Tononi,
698 G. (2009). Cortical firing and sleep homeostasis. Neuron *63*, 865–878.

699 Vyazovskiy, V.V., Olcese, U., Hanlon, E.C., Nir, Y., Cirelli, C., and Tononi, G. (2011). Local sleep in awake
700 rats. Nature *472*, 443–447.

701 Vyazovskiy, V.V., Cui, N., Rodriguez, A.V., Funk, C., Cirelli, C., and Tononi, G. (2014). The dynamics of
702 cortical neuronal activity in the first minutes after spontaneous awakening in rats and mice. Sleep *37*,
703 1337–1347.

704 Wang, X., and Michaelis, E.K. (2010). Selective neuronal vulnerability to oxidative stress in the brain.
705 Front. Aging Neurosci. *2*.

706 Watson, B.O., Levenstein, D., Greene, J.P., Gelinas, J.N., and Buzsáki, G. (2016). Network Homeostasis
707 and State Dynamics of Neocortical Sleep. ResearchGate.

708 Werth, E., Achermann, P., and Borbély, A.A. (1996). Brain topography of the human sleep EEG: antero-
709 posterior shifts of spectral power. Neuroreport *8*, 123–127.

710 Zavada, A., Strijkstra, A.M., Boerema, A.S., Daan, S., and Beersma, D.G.M. (2009). Evidence for
711 differential human slow-wave activity regulation across the brain. J Sleep Res *18*, 3–10.

712 **Figure Legends**

713 **Figure 1.** Cortical spike firing patterns are associated with the dynamics of Process S. **A)** An example of
714 the classical state-based Process S model (blue) describing the dynamics of frontal EEG SWA (median
715 per NREM sleep episode, black bars) over 48 hours in one representative animal. Sleep deprivation
716 occurred as indicated at light onset of the second day and lasted 6 hours. Scored vigilance states are also
717 shown. **B)** An example of frontal electroencephalogram (EEG), primary motor cortical local field
718 potentials (LFP), corresponding raw signal with multi-unit activity (MUA), and detected spikes, in
719 representative segments of waking and NREM sleep. Slow waves and synchronous spiking off periods
720 are visible in NREM sleep but not wakefulness. **C)** The distribution of mean firing rate during wake,
721 NREM and REM sleep over the whole dataset, in addition to the difference in mean firing rate in wake
722 compared to NREM sleep (all are positive, reflecting higher firing in wake). Points indicate channels
723 grouped by animal (left to right), but boxplots reflect channels from all animals treated as a single
724 population. **D)** Distribution of correlation coefficients, calculated within each single channel, between
725 wake episode duration (Duration), the change in slow wave activity (dSWA), and mean firing rate (mean
726 FR). Points indicate channels grouped by animal (left to right), but boxplots reflect channels from all
727 animals treated as a single population. **E)** An example scatter plot of the correlation between the change
728 in median SWA from one NREM episode to the next and the mean firing rate during the intervening
729 period of wakefulness. This channel is representative because it has the median correlation coefficient
730 of all channels.

731 **Figure 2.** Slow wave activity dynamics at the LFP level can be modelled using multi-unit spiking
732 information. **A)** An example from one representative animal modelling the SWA averaged over all LFP
733 channels, of both the classical model (blue) and novel firing-rate-based model (orange), calculated from
734 the firing rate also averaged over all LFP channels (brown). **B)** An example of both models applied to
735 the SWA of a single LFP channel, which came from the same animal as used in **A**.

736 **Figure 3.** The fit quality and parameters for both classical and firing-rate-based models of LFP SWA. **A)**
737 Equations for the classic state-based model (blue) and novel firing-rate-based model (orange). **B)** For
738 each animal, the distribution over channels of the median difference between the model and empirical

739 SWA, expressed as a percentage of empirical SWA, for both classic and firing-rate-based models. **C)** The
740 same median percent error, grouped over animals and models, separately showing errors at the level of
741 single LFP, averaged LFP and EEG. **D-G)** The distribution of values used for each parameter in the classic
742 model and **H-L)** in the firing-rate-based model, with boxplots plotted separately for each animal. The
743 black lines indicate the values obtained from modelling the averaged LFP SWA and firing rate over all
744 channels within an animal. Additionally, the red lines in **D-G** give the parameter value obtained from the
745 model of the frontal EEG SWA of that animal. **M)** The distribution of the final optimised value for the
746 firing rate set point parameter ($\boldsymbol{F_\theta}$) of the firing-rate-based model, z-normalised to the distribution of
747 firing rates within wake, NREM and REM sleep. Points indicate channels grouped by animal (left to
748 right), but boxplots reflect all channels treated as a single population. **N)** The distribution of mean firing
749 rate in wake, NREM and REM sleep, expressed as a percentage of the firing rate set point parameter ($\boldsymbol{F_\theta}$).
750 Points indicate channels grouped and coloured by animal, but boxplots reflect all channels treated as a
751 single population. **O)** The distribution of values of the change in Process S ($\boldsymbol{\Delta S/\Delta t}$) from one 4-second
752 time step to the next derived from the Fr-SWA model in wake, NREM sleep and REM sleep. All mice,
753 channels and time are pooled.

754 **Figure 4.** The definition of off periods and off occupancy. **A)** An example section of LFP (raw in grey,
755 0.5-6Hz filtered in black) and simultaneous MUA spikes. During this time window, the filtered LFP
756 crosses the amplitude threshold (265 μV for this channel, red line) five times. The multi-unit inter-spike
757 interval aligned to two of these peaks exceeds the duration threshold (85ms for this channel) and so
758 two off periods are detected (grey boxes). ISIs aligned to the other three out of five crossings (asterisks)
759 are too short to be considered off periods. **B)** Histograms of multi-unit inter-spike intervals aligned with
760 detected slow waves for this example channel. The four plots show, from left to right, ISIs over the whole
761 recording and separately ISIs from wake, NREM and REM sleep only. The ISI duration threshold (red
762 line) is selected using the histogram of all ISIs (leftmost) at the minimum between the two modes. **C)**
763 The distribution of LFP amplitude and **D)** ISI duration threshold values used for definition of off periods
764 for each channel, with boxplots plotted separately for each animal. **E)** The mean multi-unit firing rate
765 over a 1-second period centred on the peak of detected slow waves, calculated over all slow waves
766 within one example channel with 1-millisecond resolution. **F)** Distributions of mean off occupancy (%)

767 for all channels averaged over wake, NREM and REM sleep. Points indicate channels grouped by animal
768 (left to right), but boxplots reflect all channels treated as a single population. **G)** Off occupancy is shown
769 alongside EEG and LFP SWA for an example channel over 48 hours. Traces represent these values
770 calculated at 4-second resolution (light grey), in addition to the median value per NREM sleep episode,
771 as used for model fitting (black bars). Firing rate (brown) and scored vigilance states are also shown.

772 **Figure 5.** Process S is reflected in an LFP channel's off occupancy and its dynamics are described well
773 by both state-based and firing-rates-based models. **A)** An example of the novel model based on firing
774 rates and off occupancy (purple), and the classic state-based model (blue), with optimised parameters
775 describing the dynamics of off occupancy (median per NREM episode, black bars) over 48 hours. Sleep
776 deprivation occurred as indicated at light onset of the second day and lasted 6 hours. Firing rate
777 (brown), off occupancy (value per 4-second epoch, grey) and scored vigilance states are also shown. **B)**
778 Equations for the classic state based model (blue) and firing-rate-and-off-occupancy-based model for
779 off occupancy (purple). **C)** For each animal, the distribution over channels of the median difference
780 between the model and empirical off occupancy, expressed as a percentage of the off occupancy, for both
781 classic and firing-rate-based models. **D)** The distribution of values of the change in Process S ($\boldsymbol{\Delta S/\Delta t}$)
782 from one 4-second time step to the next derived from the Fr-SWA model in wake, NREM sleep and REM
783 sleep. All mice, channels and time are pooled. **E-H)** The distribution of optimised values used for each
784 parameter in the classic model and **I-L)** the firing rate model, with boxplots plotted separately for each
785 animal.

786 **Figure 6.** The time course of Process S is similar between models and individual channels. Process S
787 time courses, expressed for each channel as a percentage of the maximum value, overlaid for all channels
788 within a single representative animal obtained from **A)** the classic state-based model applied to LFP
789 SWA, **B)** the firing-rate-based model applied to LFP SWA, **C)** the classic state-based model applied to off
790 occupancy, **D)** the firing-rate-based model applied to off occupancy. In these panels the black line
791 indicates the mean Process S over all channels. **E)** The mean Process S calculated over all channels is
792 now plotted in colour (Cl-SWA light blue, Fr-SWA orange, Cl-Off dark blue, Fr-Off purple), and the red
793 line indicates the Process S obtained by applying model Cl-SWA to the EEG derived SWA.

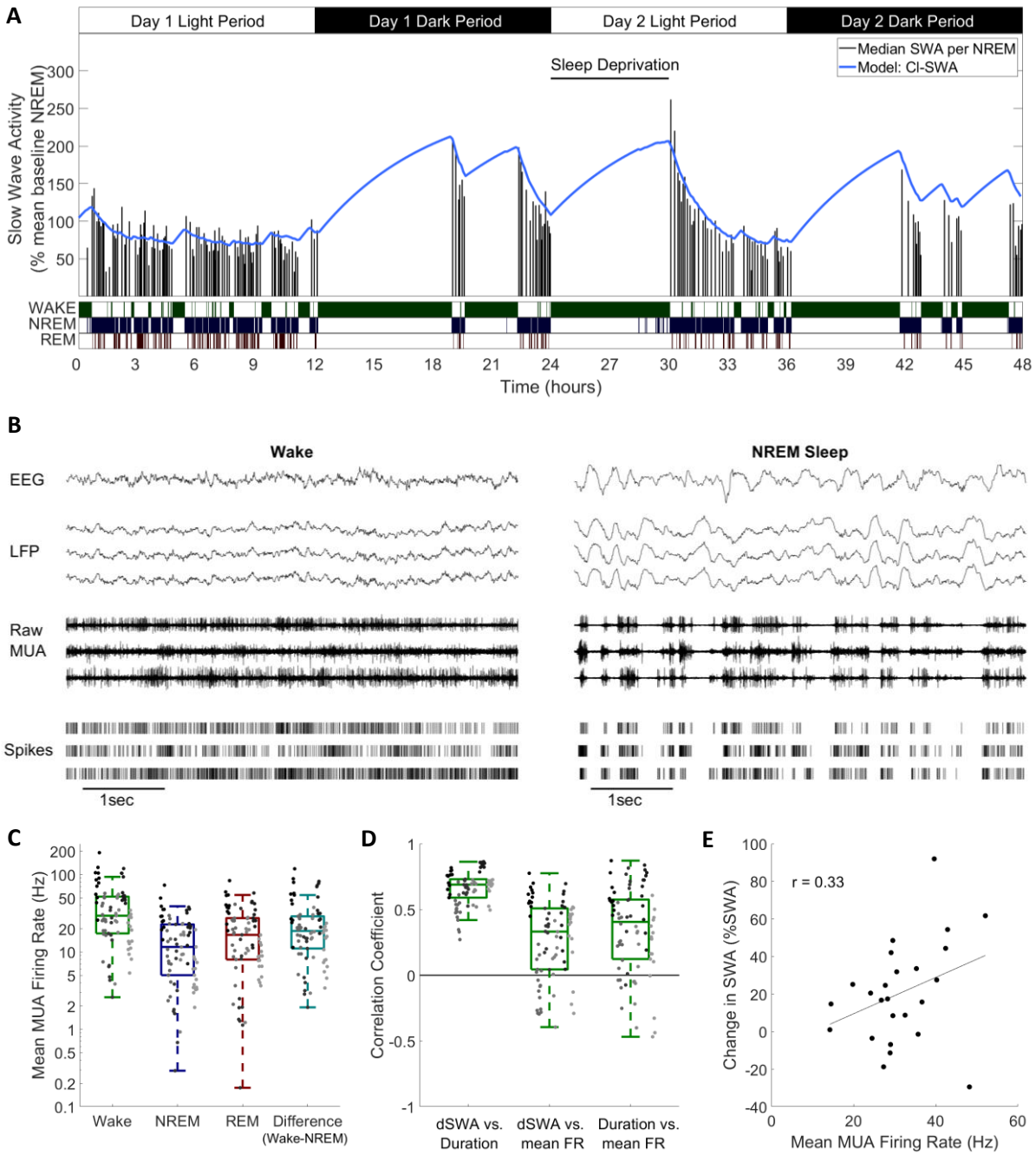
A
Day 1 Light Period
Day 1 Dark Period
Day 2 Light Period
Day 2 Dark Period
Sleep Deprivation
Median SWA per NREM
Model: CI-SWA
Slow Wave Activity (% mean baseline NREM)
WAKE
NREM
REM
Time (hours)
B
Wake
NREM Sleep
EEG
LFP
Raw
MUA
Spikes
1sec
C
Mean MUA Firing Rate (Hz)
Wake
NREM
REM
Difference (Wake-NREM)
D
Correlation Coefficient
dSWA vs. Duration
dSWA vs. mean FR
Duration vs. mean FR
E
r = 0.33
Change in SWA (%SWA)
Mean MUA Firing Rate (Hz)

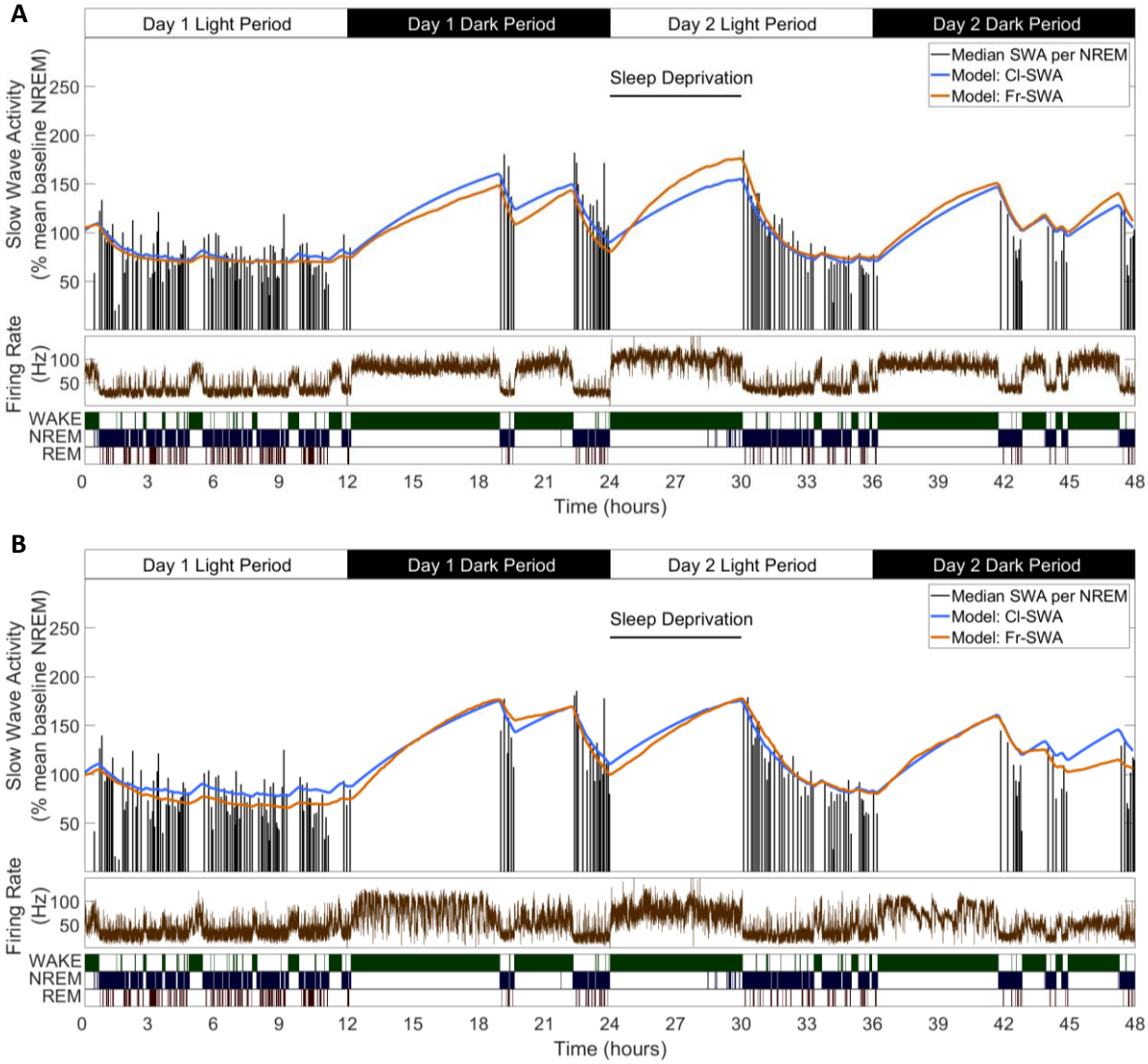
A
Day 1 Light Period
Day 1 Dark Period
Day 2 Light Period
Day 2 Dark Period
Sleep Deprivation
Median SWA per NREM
Model: Cl-SWA
Model: Fr-SWA
Slow Wave Activity
(% mean baseline NREM)
Firing Rate
(Hz)
WAKE
NREM
REM
Time (hours)
B
Day 1 Light Period
Day 1 Dark Period
Day 2 Light Period
Day 2 Dark Period
Sleep Deprivation
Median SWA per NREM
Model: Cl-SWA
Model: Fr-SWA
Slow Wave Activity
(% mean baseline NREM)
Firing Rate
(Hz)
WAKE
NREM
REM
Time (hours)

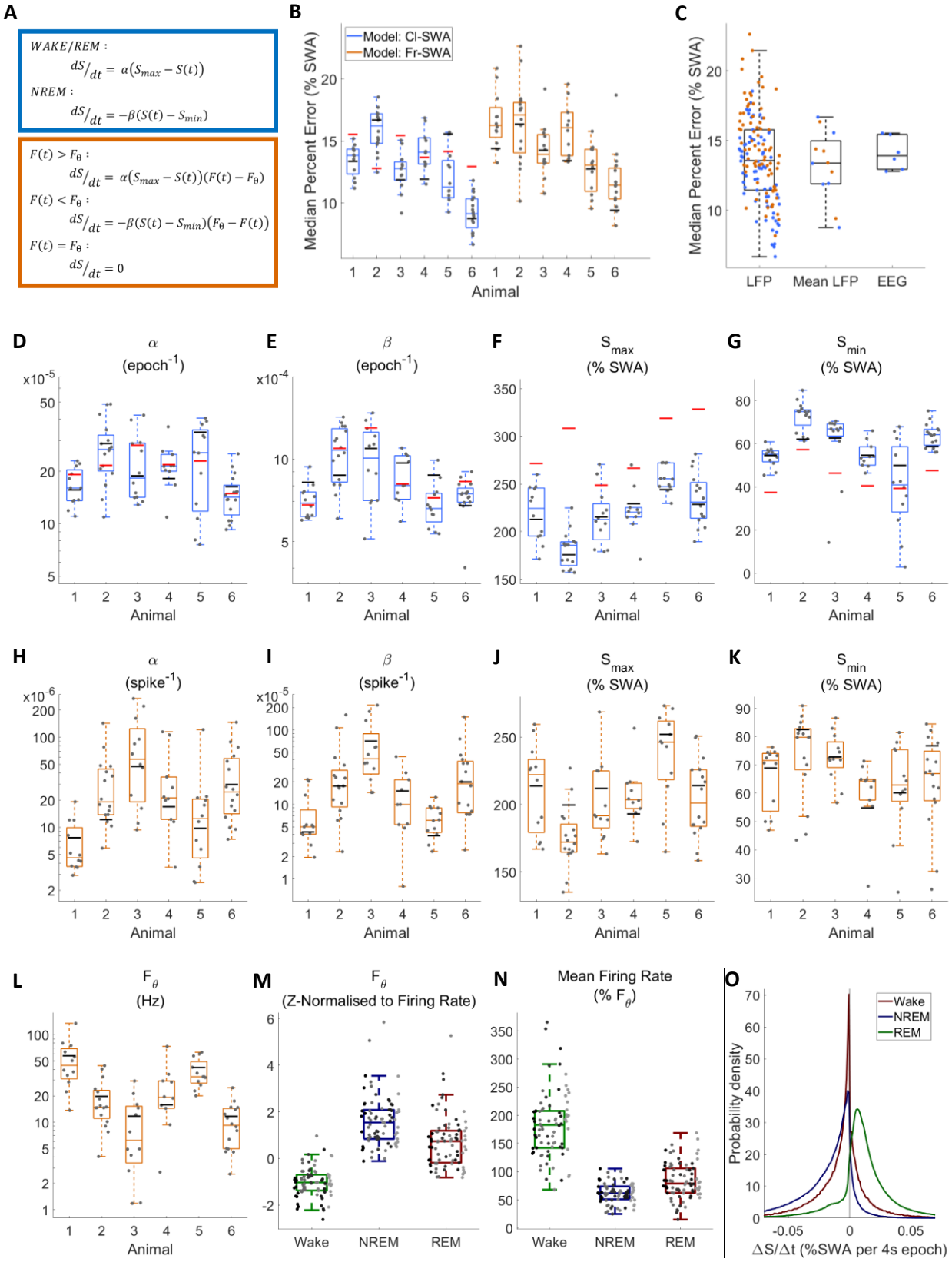
A
WAKE/REM :
$dS/dt = \alpha(S_{max} - S(t))$
NREM :
$dS/dt = -\beta(S(t) - S_{min})$
$F(t) > F_\theta$:
$dS/dt = \alpha(S_{max} - S(t))(F(t) - F_\theta)$
$F(t) < F_\theta$:
$dS/dt = -\beta(S(t) - S_{min})(F_\theta - F(t))$
$F(t) = F_\theta$:
$dS/dt = 0$
B
Model: Cl-SWA
Model: Fr-SWA
Median Percent Error (% SWA)
Animal
C
Median Percent Error (% SWA)
LFP
Mean LFP
EEG
D
α (epoch^{-1})
E
β (epoch^{-1})
F
S_{max} (% SWA)
G
S_{min} (% SWA)
H
α (spike^{-1})
I
β (spike^{-1})
J
S_{max} (% SWA)
K
S_{min} (% SWA)
L
F_θ (Hz)
M
F_θ (Z-Normalised to Firing Rate)
N
Mean Firing Rate (% F_θ)
Wake
NREM
REM
O
Probability density
ΔS/Δt (%SWA per 4s epoch)

Figure 3

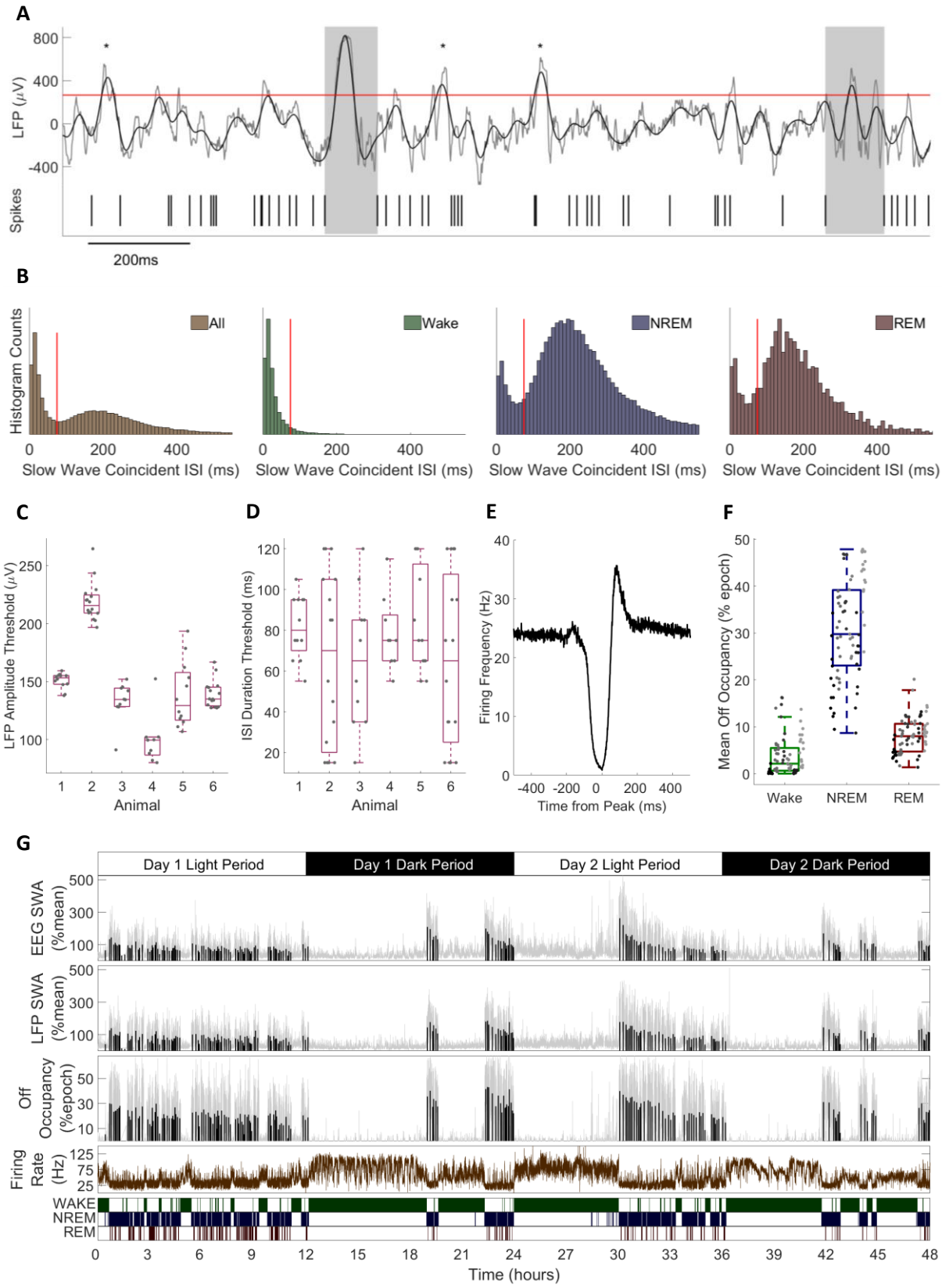
A
LFP (μV)
Spikes
200ms
B
Histogram Counts
All
Wake
NREM
REM
Slow Wave Coincident ISI (ms)
C
LFP Amplitude Threshold (μV)
Animal
D
ISI Duration Threshold (ms)
Animal
E
Firing Frequency (Hz)
Time from Peak (ms)
F
Mean Off Occupancy (% epoch)
Wake
NREM
REM
G
Day 1 Light Period
Day 1 Dark Period
Day 2 Light Period
Day 2 Dark Period
EEG SWA (%mean)
LFP SWA (%mean)
Off Occupancy (%epoch)
Firing Rate (Hz)
WAKE
NREM
REM
Time (hours)

Figure 4

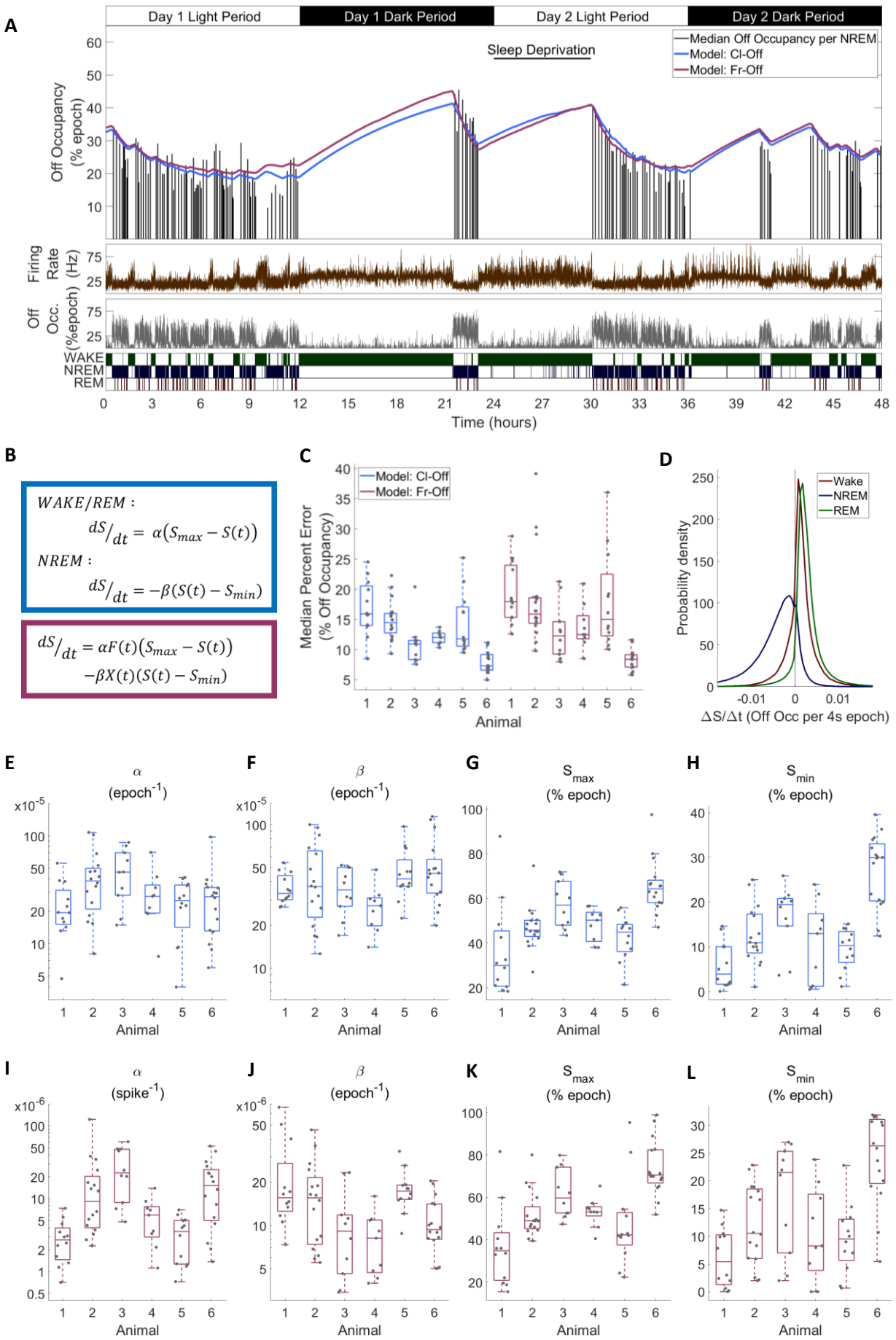
A
Day 1 Light Period
Day 1 Dark Period
Day 2 Light Period
Day 2 Dark Period
Sleep Deprivation
Median Off Occupancy per NREM
Model: Cl-Off
Model: Fr-Off
Off Occupancy (% epoch)
Firing Rate (Hz)
Off Occ. (%epoch)
WAKE
NREM
REM
Time (hours)
B
WAKE/REM :
$dS/dt = \alpha(S_{max} - S(t))$
NREM :
$dS/dt = -\beta(S(t) - S_{min})$
$dS/dt = \alpha F(t)(S_{max} - S(t)) - \beta X(t)(S(t) - S_{min})$
C
Model: Cl-Off
Model: Fr-Off
Median Percent Error (% Off Occupancy)
Animal
D
Wake
NREM
REM
Probability density
ΔS/Δt (Off Occ per 4s epoch)
E
α (epoch^{-1})
F
β (epoch^{-1})
G
S_{max} (% epoch)
H
S_{min} (% epoch)
I
α (spike^{-1})
J
β (epoch^{-1})
K
S_{max} (% epoch)
L
S_{min} (% epoch)
Animal

Figure 5

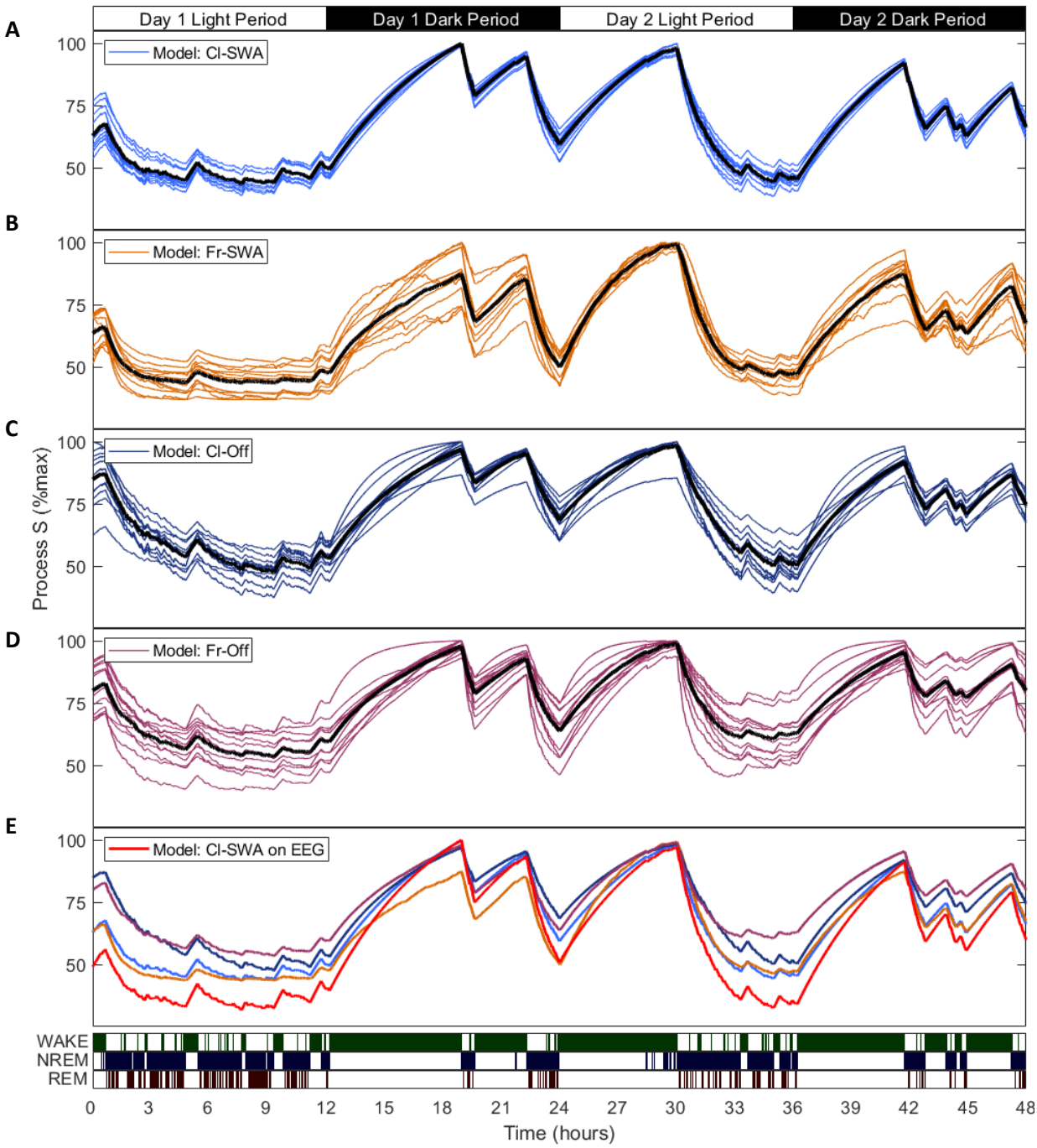
Day 1 Light Period
Day 1 Dark Period
Day 2 Light Period
Day 2 Dark Period
A
Model: Cl-SWA
B
Model: Fr-SWA
C
Model: Cl-Off
D
Model: Fr-Off
E
Model: Cl-SWA on EEG
Process S (%max)
100
75
50
WAKE
NREM
REM
0
3
6
9
12
15
18
21
24
27
30
33
36
39
42
45
48
Time (hours)

Figure 6